

# Efficient method to suppress artifacts caused by tissue hyper-reflections in optical microangiography of retina in vivo

Yanping Huang, Qinqin Zhang, and Ruikang K. Wang\*

Department of Bioengineering, University of Washington, 3720 15th NE, Seattle, WA 98195, USA  
\*wangrk@uw.edu

**Abstract:** Optical microangiography (OMAG) is an optical coherence tomography (OCT)-based imaging technique that is capable of achieving the angiographic imaging of biological tissues in vivo with a high imaging resolution and no need for dye injection. OMAG has a potential to become a clinical tool for the diagnosis and treatment monitoring of various retinopathies. In principle, OMAG extracts blood flow information based on a direct differentiation of complex or intensity OCT signals between repeated B-scans acquired at the same cross section, which is sensitive to blood cell movement. In practice, this method is prone to artifacts due to tissue hyper-reflection, commonly seen in retinal diseases such as diabetic retinopathy. In this paper, we propose a novel method to suppress the artifacts induced by hyper-reflection. We propose to scale OMAG flow signals by a weighting factor that is motion-sensitive but hyper-reflection insensitive. We show that this simple weighting approach is effective in suppressing the artifacts due to tissue hyper-reflections while still maintaining the detected capillary networks with high fidelity, especially in deeper retina. The effectiveness of the proposed technique is demonstrated by a phantom study and case studies on patients' eyes with hyper-reflective foci. Finally we discuss potential applications of this technique.

©2015 Optical Society of America

**OCIS codes:** (170.4500) Optical coherence tomography; (170.2655) Functional monitoring and imaging; (170.1470) Blood or tissue constituent monitoring.

## References and links

1. T. Bek, "Regional morphology and pathophysiology of retinal vascular disease," *Prog. Retin. Eye Res.* **36**, 247–259 (2013).
2. K. R. Mendis, C. Balaratnasingam, P. Yu, C. J. Barry, I. L. McAllister, S. J. Cringle, and D. Y. Yu, "Correlation of histologic and clinical images to determine the diagnostic value of fluorescein angiography for studying retinal capillary detail," *Invest. Ophthalmol. Vis. Sci.* **51**(11), 5864–5869 (2010).
3. Z. Popovic, P. Knutsson, J. Thaug, M. Owner-Petersen, and J. Sjöstrand, "Noninvasive imaging of human foveal capillary network using dual-conjugate adaptive optics," *Invest. Ophthalmol. Vis. Sci.* **52**(5), 2649–2655 (2011).
4. J. Tam, K. P. Dhamdhere, P. Tiruveedhula, S. Manzanera, S. Barez, M. A. Bearse, Jr., A. J. Adams, and A. Roorda, "Disruption of the retinal parafoveal capillary network in type 2 diabetes before the onset of diabetic retinopathy," *Invest. Ophthalmol. Vis. Sci.* **52**(12), 9257–9266 (2011).
5. Z. P. Chen, T. E. Milner, S. Srinivas, X. J. Wang, A. Malekafzali, M. J. C. van Gemert, and J. S. Nelson, "Noninvasive imaging of in vivo blood flow velocity using optical Doppler tomography," *Opt. Lett.* **22**(14), 1119–1121 (1997).
6. R. K. Wang and Z. Ma, "Real-time flow imaging by removing texture pattern artifacts in spectral-domain optical Doppler tomography," *Opt. Lett.* **31**(20), 3001–3003 (2006).
7. R. A. Leitgeb, L. Schmetterer, W. Drexler, A. F. Fercher, R. J. Zawadzki, and T. Bajraszewski, "Real-time assessment of retinal blood flow with ultrafast acquisition by color Doppler Fourier domain optical coherence tomography," *Opt. Express* **11**(23), 3116–3121 (2003).
8. B. R. White, M. C. Pierce, N. Nassif, B. Cense, B. H. Park, G. J. Tearney, B. E. Bouma, T. C. Chen, and J. F. de Boer, "In vivo dynamic human retinal blood flow imaging using ultra-high-speed spectral domain optical coherence tomography," *Opt. Express* **11**(25), 3490–3497 (2003).

9. R. K. Wang, "Method and Apparatus for Ultrahigh Sensitive Optical Microangiography". Patent Identification. No. 20120307014 (2010).
10. J. K. Barton and S. Stromski, "Flow measurement without phase information in optical coherence tomography images," *Opt. Express* **13**(14), 5234–5239 (2005).
11. C. Blatter, T. Klein, B. Grajciar, T. Schmoll, W. Wieser, R. Andre, R. Huber, and R. A. Leitgeb, "Ultrahigh-speed non-invasive widefield angiography," *J. Biomed. Opt.* **17**(7), 070505 (2012).
12. A. Mariampillai, B. A. Standish, E. H. Moriyama, M. Khurana, N. R. Munce, M. K. K. Leung, J. Jiang, A. Cable, B. C. Wilson, I. A. Vitkin, and V. X. D. Yang, "Speckle variance detection of microvasculature using swept-source optical coherence tomography," *Opt. Lett.* **33**(13), 1530–1532 (2008).
13. J. Fingler, D. Schwartz, C. H. Yang, and S. E. Fraser, "Mobility and transverse flow visualization using phase variance contrast with spectral domain optical coherence tomography," *Opt. Express* **15**(20), 12636–12653 (2007).
14. D. Y. Kim, J. Fingler, R. J. Zawadzki, S. S. Park, L. S. Morse, D. M. Schwartz, S. E. Fraser, and J. S. Werner, "Optical imaging of the chorioretinal vasculature in the living human eye," *Proc. Natl. Acad. Sci. U.S.A.* **110**(35), 14354–14359 (2013).
15. R. K. Wang, S. L. Jacques, Z. Ma, S. Hurst, S. R. Hanson, and A. Gruber, "Three dimensional optical angiography," *Opt. Express* **15**(7), 4083–4097 (2007).
16. Z. W. Zhi, J. Qin, L. An, and R. K. K. Wang, "Supercontinuum light source enables in vivo optical microangiography of capillary vessels within tissue beds," *Opt. Lett.* **36**(16), 3169–3171 (2011).
17. R. K. Wang, L. An, P. Francis, and D. J. Wilson, "Depth-resolved imaging of capillary networks in retina and choroid using ultrahigh sensitive optical microangiography," *Opt. Lett.* **35**(9), 1467–1469 (2010).
18. L. An, H. M. Subhush, D. J. Wilson, and R. K. Wang, "High-resolution wide-field imaging of retinal and choroidal blood perfusion with optical microangiography," *J. Biomed. Opt.* **15**(2), 026011 (2010).
19. R. K. Wang, L. An, S. Saunders, and D. J. Wilson, "Optical microangiography provides depth-resolved images of directional ocular blood perfusion in posterior eye segment," *J. Biomed. Opt.* **15**(2), 020502 (2010).
20. P. A. Keane and S. R. Sadda, "Imaging chorioretinal vascular disease," *Eye (Lond.)* **24**(3), 422–427 (2010).
21. L. An, T. T. Shen, and R. K. K. Wang, "Using ultrahigh sensitive optical microangiography to achieve comprehensive depth resolved microvasculature mapping for human retina," *J. Biomed. Opt.* **16**(10), 106013 (2011).
22. Y. P. Huang, Q. Q. Zhang, M. R. Thorell, L. An, M. K. Durbin, M. Laron, G. Gregori, U. Sharma, P. J. Rosenfeld, and R. K. Wang, "Swept-source OCT angiography of the retinal vasculature using intensity differentiation based OMAG algorithms," *OSLI Retina*. **45**(5), 382–389 (2014).
23. M. R. Thorell, Q. Q. Zhang, Y. P. Huang, L. An, M. K. Durbin, M. Laron, U. Sharma, P. F. Stetson, G. Gregori, R. K. Wang, and P. J. Rosenfeld, "Swept-source OCT angiography of macular telangiectasia type 2," *Ophthalmic Surg Lasers Imaging Retina* **45**(5), 369–380 (2014).
24. M. Bolz, U. Schmidt-Erfurth, G. Deak, G. Mylonas, K. Kriechbaum, and C. Scholda; Diabetic Retinopathy Research Group Vienna, "Optical coherence tomographic hyperreflective foci: a morphologic sign of lipid extravasation in diabetic macular edema," *Ophthalmology* **116**(5), 914–920 (2009).
25. A. Uji, T. Murakami, K. Nishijima, T. Akagi, T. Horii, N. Arakawa, Y. Muraoka, A. A. Ellabban, and N. Yoshimura, "Association between hyperreflective foci in the outer retina, status of photoreceptor layer, and visual acuity in diabetic macular edema," *Am. J. Ophthalmol.* **153**(4), 710–717 (2012).
26. G. Coscas, U. De Benedetto, F. Coscas, C. I. Li Calzi, S. Vismara, F. Roudot-Thoraval, F. Bandello, and E. Souied, "Hyperreflective dots: a new spectral-domain optical coherence tomography entity for follow-up and prognosis in exudative age-related macular degeneration," *Ophthalmologica* **229**(1), 32–37 (2013).
27. J. M. Schmitt, S. H. Xiang, and K. M. Yung, "Speckle in optical coherence tomography," *J. Biomed. Opt.* **4**(1), 95–105 (1999).
28. U. Baran, L. Shi, and R. K. Wang, "Capillary blood flow imaging within human finger cuticle using optical microangiography," *J. Biophotonics*, **8**, 46–51 (2013).
29. R. Motaghiannezam and S. Fraser, "Logarithmic intensity and speckle-based motion contrast methods for human retinal vasculature visualization using swept source optical coherence tomography," *Biomed. Opt. Express* **3**(3), 503–521 (2012).
30. J. Enfield, E. Jonathan, and M. Leahy, "In vivo imaging of the microcirculation of the volar forearm using correlation mapping optical coherence tomography (cmOCT)," *Biomed. Opt. Express* **2**(5), 1184–1193 (2011).
31. Y. Wang and R. K. Wang, "Autocorrelation optical coherence tomography for mapping transverse particle-flow velocity," *Opt. Lett.* **35**(21), 3538–3540 (2010).
32. W. J. Choi, R. Reif, S. Yousefi, and R. K. Wang, "Improved microcirculation imaging of human skin in vivo using optical microangiography with a correlation mapping mask," *J. Biomed. Opt.* **19**(3), 036010 (2014).
33. G. Wagnières, S. G. Cheng, M. Zellweger, N. Utke, D. Braichotte, J. P. Ballini, and H. van den Bergh, "An optical phantom with tissue-like properties in the visible for use in PDT and fluorescence spectroscopy," *Phys. Med. Biol.* **42**(7), 1415–1426 (1997).
34. X. Yin, J. R. Chao, and R. K. Wang, "User-guided segmentation for volumetric retinal optical coherence tomography images," *J. Biomed. Opt.* **19**(8), 086020 (2014).
35. G. G. Deák, M. Bolz, K. Kriechbaum, S. Prager, G. Mylonas, C. Scholda, and U. Schmidt-Erfurth; Diabetic Retinopathy Research Group Vienna, "Effect of retinal photocoagulation on intraretinal lipid exudates in

- diabetic macular edema documented by optical coherence tomography,” *Ophthalmology* **117**(4), 773–779 (2010).
36. S. Baumüller, P. Charbel Issa, H. P. N. Scholl, S. Schmitz-Valckenberg, and F. G. Holz, “Outer retinal hyperreflective spots on spectral-domain optical coherence tomography in macular telangiectasia type 2,” *Ophthalmology* **117**(11), 2162–2168 (2010).
- 

## 1. Introduction

Retinal microcirculation is of critical importance in maintaining normal visual functions for the eye. Physiologically, retinal microcirculation provides sufficient oxygen and nutrients to and removes metabolites and wastes from active retinal tissue, maintaining a delicate balance between demand and supply. However, the vascular network would be altered in a majority of retinal pathologies, which could affect photoreceptor function leading to a significant loss of vision [1]. Therefore, it is important to develop clinical tools that can directly visualize the changes in retinal vasculature in a scale down to capillary level.

Fluorescein angiography (FA), as a minimally invasive method, has been treated as the *de facto* gold standard for the clinical investigation and diagnosis of the vascular change in retina. Vascular pathologies such as ischemia and degraded blood-retinal barrier can be detected based on the observations of dynamic FA images after dye injection. However, due to its relatively low spatial resolution and lack of depth information, it is difficult to obtain detailed information of the pathology such as the location of affected vessels and the specific morphological changes in capillary network [2]. Most recently, adaptive optics scanning laser ophthalmoscope (AOSLO) based high resolution imaging method has been explored for the finer imaging and quantification of capillary network in retina [3,4]. However, relatively strict experimental conditions such as subject fixation, small field of view and high cost for imaging system, have limited its applications mainly to laboratory and investigational research.

Optical coherence tomography (OCT) is a high resolution imaging modality that can be used for both structural and functional imaging of the posterior eye. OCT has been demonstrated to be a potential tool to study the retinal blood flow based on the principle of Doppler phenomenon [5–8]. However, Doppler based flow detection is dependent on the Doppler angle, which is intrinsically insensitive to the particle movement perpendicular to the probing beam. Most of the retinal blood vessels are running in parallel to the retinal surface that are almost perpendicular to the incident OCT probe beam, leading to a difficulty in detecting retinal blood flows using Doppler principle.

In addition to velocity measurement by the direct use of phase changes in OCT signals, angiographic imaging can also be achieved using other contrast mechanisms. Recently, a prevalent scanning protocol called B-M scan [9], i.e., repeated B-scans at the same location, has been utilized to detect the functional vasculature innervated within biological tissues in vivo. The basic principle is to evaluate inter-frame difference as the mechanism of contrast to differentiate functional blood flows from static structures. In terms of computational methods, OCT-based angiography can be generated using the variations of repeated measurements in OCT intensity [10–12], phase [13,14] or combined complex signals [15–19]. This method has shown clinical promise particularly for retinal imaging compared to conventional FA because it is noninvasive and utilizes endogenous contrast without a need for dye injection [20].

Optical microangiography (OMAG) is an OCT-based angiography technique to study microcirculation perfused within tissue beds, which has been successfully applied to extract retinal vasculature networks [17,18,21]. A direct subtraction of complex or intensity OCT signals between repeated B-scans is used to extract the blood flow signal in OMAG. Such simple differentiation operation is demonstrated very sensitive in the detection of capillary networks of retina in both normal subjects and patients [22,23]. In repeated B-scans, the appearance of different physiological layers in retina is relatively homogeneous and stable except those parts occupied by functional blood vessels. However, in preliminary clinical study it is found that this method is prone to artifacts caused by hyper-reflective signals from

some hyper-reflective foci located at specific retinal layers such as hard exudates in patients with diabetic retinopathy (DR) [24,25] or pigment migration in age-related macular degeneration (AMD) [26]. OCT speckle is multiplicative in nature [27]. Therefore, any fluctuation in the OCT signals due to hyper-reflective static structures will induce a large change in its absolute value, leading to flow artifacts in OMAG. In normal subjects, a multi-layered structure can be clearly observed in the OCT images of a retina, with higher reflection mainly coming from the nerve fiber layer (NFL), photoreceptor inner segment (IS)/outer segment (OS) interface, and retinal pigment epithelium (RPE). These high reflective layers lead to noticeable artifacts in the OMAG images that degrade the visibility of blood vessels in enface projection images. These artifacts in normal subjects can be excluded with ease from the final angiographic enface images by the use of layer segmentation algorithms. However, when the hyper-reflection is irregularly scattered in space within retina, it is difficult, if not impossible to remove the associated artifacts in OMAG by segmentation algorithms. On the one hand, the hyper-reflection can be recognized as clear symptoms of the disease itself such as a degraded blood-retinal barrier so they may not completely meaningless. On the other hand, they should be suppressed if the aim of study is to detect the change in the true vasculature network itself.

In order to suppress the artifacts caused by hyper-reflection in retinal vasculature OMAG images, we propose a method that utilizes a motion index parameter, such as decorrelation coefficient, as an independent weighting variable to scale the resulted OMAG signals. For the sake of brevity, we term this method as weighted OMAG (wOMAG). The remaining parts of this paper are arranged as follows: OCT systems and scanning protocols are first introduced briefly, followed by the details of the processing methods for OMAG and proposed wOMAG. The effectiveness of the proposed technique in suppressing the hyper-reflective artifacts is then tested using a purposely designed phantom experiment, as well as through two case studies with hyper-reflective foci in patients with identified retinal pathologies. Finally, the results of the current study and potential applications of the proposed method are discussed.

## **2. Material and methods**

### *2.1. OCT system and scanning protocols*

A modified Cirrus HD 5000 spectral domain OCT system (Carl Zeiss Meditec Inc., Dublin, CA, USA) with 68 kHz A-line acquisition speed and a central wavelength of 842 nm was used in this study for retinal scanning. In the system, the scanning protocol provides a field of view of either  $2.4 \times 2.4 \text{ mm}^2$  or  $3 \times 3 \text{ mm}^2$  with 245 lines in the fast scan direction (B-mode) and 245 frames in the slow scan axis. To enable OMAG, a repeated B-scan scanning protocol is adopted, i.e., B-scans are repeated four times at each slow scan position to extract the flow signal [17,28]. The time duration for a whole 3D cube scan is  $\sim 3.5$  s, which is acceptable for a typical patient study in clinical situations. More detailed description for the scanning protocols can be found in a previous publication [22].

Recognizing that the phantom study requires a different setup from the ocular optical system, another custom-designed 92 kHz spectral domain OCT system with a central wavelength of 1340 nm was employed with the same scanning protocols as in the human imaging case. Four repeated scans were performed at the same cross-section to extract “blood flow” information. More details of this system can be found in [28].

### *2.2. Proposed algorithm of weighted OMAG*

The complex OCT signals were firstly obtained by fast Fourier transformation of the dispersion-compensated k-space spectral data. Before applying algorithms for OCT angiography, large bulk motion between two repeated B-scans at each position was removed by a block matching method using cross-correlation as a searching criterion (using a phase compensation algorithm [21] if complex signal is used). An OMAG algorithm based on the

complex [17] or intensity [22] signal differentiation can be used to extract the blood flow signal. Considering the requirement of efficient computation and less storage for potential real time clinical applications, the intensity-based approach was used in the current study:

$$F_{OMAG}(x, z) = \frac{1}{R-1} \sum_{i=1}^{R-1} |I_{i+1}(x, z) - I_i(x, z)| \quad (1)$$

where  $I$  is the OCT intensity signal,  $R$  is the number of repeated B-scans at each position ( $R = 4$  in the current study),  $i$  indicates the  $i^{th}$  repeated B-scan and  $(x, z)$  is the coordinate in the fast scanning direction (the specific A-line in a B-mode image) and the depth direction, respectively. The calculated flow signal was finally log-compressed with a proper threshold (typically 3dB above noise floor) for image display.

Although OMAG is quite sensitive to detect vascular networks, including capillaries, it is prone to artifacts due to strong signals from highly reflecting structures. To mitigate this problem, we propose a weighted OMAG (wOMAG) algorithm to suppress these artifacts. wOMAG is defined as the original OMAG flow signal multiplied by a weighting factor that uses a motion index (MI) as the control variable:

$$F_{wOMAG}(x, z) = F_{OMAG}(x, z) \cdot f(MI(x, z)) \quad (2)$$

where the weighting factor  $f$  is a monotonic function of the MI. In this study we used the inter-frame pixel decorrelation coefficient (DCC) as the MI to scale the OMAG flow signals:

$$MI(x, z) = D(x, z) = \frac{1}{R-1} \sum_{i=1}^{R-1} \frac{(I_{i+1}(x, z) - I_i(x, z))^2}{I_{i+1}^2(x, z) + I_i^2(x, z)} \quad (3)$$

where  $D$  is the decorrelation coefficient. For the scaling factor, different forms of functions may be selected with respect to the independent variable, such as exponential, power or sinusoidal functions. It is empirically set as the following power form in the current study:

$$f(D) = \left( \frac{D}{D_0} \right)^n \quad (4)$$

where  $D$  is the DCC for each pixel and  $D_0$  is a threshold value for scaling. In this study, a threshold of  $D_0 = 0.1$ ,  $n = 1$  was used to generate the wOMAG retinal images in order to maximally preserve the visibility and connectivity (smoothness) of capillaries but reject the false signals due to hyper-reflective static tissues. The effects of different  $D_0$  (0.05, 0.1, 0.2, 0.4) at a fixed  $n = 1$  and of different  $n$  (0.5, 1, 2, 3) at a fixed  $D_0 = 0.1$  on the quality of vascular image are also evaluated.

For comparison, we also computed OCT angiographic images of the retinal vasculature with two existing algorithms. The first algorithm for comparison (CA1) calculates the variance based on the log-compressed intensity signal ( $LI = \log I$ , where  $I$  is the intensity signal as defined in Eq. (1) [29]). The logarithmic operation turns a multiplicative noise into an additive noise so it is less sensitive to the intensity-induced artifacts [29]:

$$F_{CA1}(x, z) = \frac{1}{R} \sum_{i=1}^R (LI_i(x, z) - \overline{LI}(x, z))^2 \quad (5)$$

where  $\overline{LI}(x, z)$  is the average log-compressed intensity for the four repeated measurements at the same point  $(x, z)$ . From the definition, this method (CA1) can be equivalently seen as a log-compressed speckle variance method. The second algorithm for comparison (CA2) is the decorrelation method and it directly uses DCC Eq. (3) as the parameter to generate vascular

image [30]. The principle is that OCT signal decorrelates along time and the decorrelation is larger at the point with fast flow than slow flow [31]. As only single point in four repeated B-scan frames was used for the calculation, the computational cost is greatly reduced in this algorithm compared to subregion-based decorrelation algorithms [30, 32]. In order to avoid inaccurate estimation from noisy background, a mask based on intensity thresholding was used to display the final image for both methods (CA1 and CA2).

### 2.3. Phantom study

An agar phantom was built to test the effectiveness of the proposed algorithm in suppressing the artifacts caused by hyper-reflection. The method used to fabricate the agar phantom was similar to that reported in the literature [33]. Milk drops were added in 2% agar solution during the preparation process to increase its optical scattering. An aluminum wire with a diameter of 1.2 mm was embedded in the phantom to simulate the hyper-reflective feature and its effect on “blood flow” detection. Note that the phantom contained no moving parts. Thus, the ideal OMAG image of this phantom should be black, i.e. no flow signal. For OCT imaging, only one cross-section was scanned. Each B-scan consisted of 256 A-lines corresponding to a scan range of 1.5 mm.

### 2.4. Case study on patients

Clinical data set were obtained from the left eye of a patient with diabetic retinopathy (DR) and the left eye of a second patient with polypoidal choroidal vasculopathy (PCV). For the DR patient, the macular region of 3 mm × 3 mm around the fovea was scanned and for the PCV patient, a temporal peripapillary region of 2.4 mm × 2.4 mm was scanned. Enface projection image was used to display the vascular networks located at different retinal layers. In this study, the retina was segmented into three layers: the inner retina from ganglion cell layer (GCL) to inner plexiform layer (IPL), the middle retina from inner nuclear layer (INL) to outer plexiform layer (OPL) and the outer retina from outer nuclear layer (ONL) to external limiting membrane (ELM) [22]. The outer retina layer is an avascular layer in normal subjects. But in pathological situations, new vessels may grow into this layer. These three layers were semi-automatically segmented based on OCT structural images using custom-written C++ coded software [34]. Fluorescein angiography (FA) of the studied region was provided here as a reference and for comparison. In the DR patient, the detailed results of OMAG and wOMAG are given in comparison with the other two OCT-based angiography methods CA1 and CA2. While in the PCV patient, only results of OMAG and wOMAG are given. The use of a modified Zeiss Cirrus HD SD-OCT prototype system for patient imaging was approved by the Institutional Review Board (IRB) of the University of Washington and consent form was obtained from each patient before examination.

## 3. Results

Figure 1 shows the results from phantom experiment. A hyper-reflective feature is clearly observed at the agar-wire interface in the structural image (Fig. 1(A)). After data processing using the intensity-based OMAG algorithm, the hyper-reflective artifacts appear in the flow image as shown in Fig. 1(B). Note that the phantom surface was adjusted oblique to the incident optical beam in order to decrease the amplitude of reflection from the air-agar interface. However, there was still some strong reflection from this interface, which also shows up as artifacts in the flow signal (Fig. 1(B)). When the same data set were processed using wOMAG, artifacts were suppressed by ~26 dB and were completely removed as shown in Fig. 1(C). This experiment demonstrates the proposed wOMAG algorithm is effective in suppressing the artifacts of OMAG induced by hyper-reflective static structures in the phantom.

For the DR patient study, two typical B frames that contain hyper-reflective foci have been selected to demonstrate how the algorithms work. The results are shown in Fig. 2. From

Fig. 2(C) and Fig. 2(D), it can be clearly observed that OMAG is very sensitive to the flow signal, but those hyper-reflective foci also show up in the image, which are regarded as the artifacts in terms of vasculature detection. The proposed wOMAG algorithm can effectively suppress these artifacts as shown in Fig. 2(E) and Fig. 2(F). For the methods CA1 and CA2, they can also suppress the hyper-reflection artifacts well and perform very similarly with each other for the typical B-frames shown in Fig. 2(G) to Fig. 2(J). However, it is noticeable that they over-suppress the flow information especially the capillaries in the deep retinal layer when compared with OMAG results. The wOMAG algorithm, on the other hand, works well to provide a better balance between the sensitive detection of capillary network and the suppression of hyper-reflective artifacts.

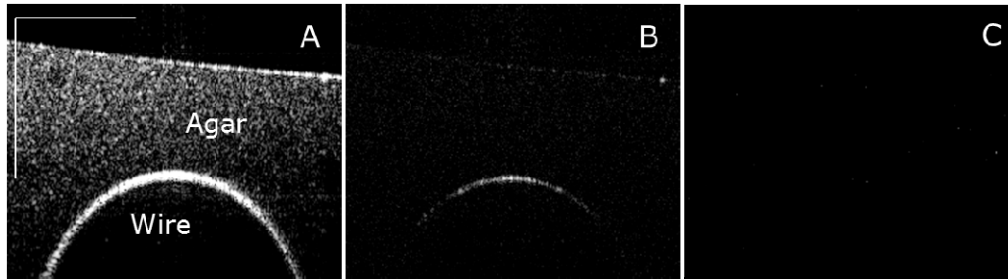


Fig. 1. (A) OCT structural image of the phantom, showing a clear hyper-reflective interface between the agar and the wire. (B) OMAG processing of the repeated measurements at this cross-section showing the artifacts of flow induced by the hyper-reflective structure. Also note some artifacts of flow from the strong reflection induced by the air-agar interface. (C) wOMAG processing of the same data set showing that the artifacts are completely suppressed. The scale bar in (A) indicates 500  $\mu\text{m}$ .

To better compare the performances of different algorithms, enface images using maximum intensity projection were generated in the three retinal layers from the scanned tissue volume and the results are shown in Fig. 3. From the OMAG enface images (Fig. 3(C1)-3(C4)), the hyper-reflective artifacts can be clearly observed in the retinal layers, especially in the middle retinal layer, as shown by patches of green in Fig. 3(C4). When viewed from the whole retinal OMAG image, the details of blood vessels can hardly be observed because of the hyper-reflection induced artifacts. For wOMAG, the artifacts induced by hyper-reflective foci have been suppressed effectively while the details of the capillary network, especially those in the deep retinal layer are seen clearly. CA1 and CA2 perform comparably with each other and they both can suppress the hyper-reflective artifacts well. However, the continuity and smoothness of the vasculature are compromised in CA1 and CA2 compared to that of OMAG and wOMAG. The degradation of vascular image quality in CA1 and CA2 is especially observed in the middle retinal layer (Fig. 3(E2) and Fig. 3(F2)) where most of the blood vessels are capillaries that are more vulnerable to pathological attack. With respect to pathological changes of the vasculature in this eye, severe capillary dropout can be clearly observed from both the inner and middle retinal layers. The OCT-based vascular images show a good correspondence with FA in terms of blood vessel distribution.

In order to observe the overall distribution of the speckle DCC for all the pixels in the scanned volume, a frequency histogram and cumulative frequency histogram were produced as shown in Fig. 4. A monotonically decreasing trend of frequency for the DCC is observed and 50% of the coefficients lie below 0.1, which most probably indicates the static part of the tissue. As shown in frequency histogram, there is no clear cutoff value of DCC that can be used as a threshold to separate the static tissue from the blood vessels. As a result, further study is conducted to show how the threshold  $D_0$  and  $n$  in the weighting factor of Eq. (4) affect the results. Figure 5 shows the results of enface wOMAG images of the whole retina

when  $D_0$  changes at four values: 0.05, 0.1, 0.2 and 0.4 while  $n = 1$  (A-D), and  $n$  changes at four values: 0.5, 1, 2 and 3 while  $D_0 = 0.1$  (E-H). The results of wOMAG are almost the same when  $D_0$  changes with a fixed  $n$ , which was found to be related to the log-compression in the display of image (see details in the Discussion section). When  $n$  increases, there is a better suppression of the hyper-reflection and the blood vessels become brighter with an increased image contrast; however, there is a loss of smoothness and connectivity of the small blood vessels, which should be avoided. It was found  $n = 1\sim 2$  is appropriate for obtaining reasonable results with satisfactory artifact suppression.

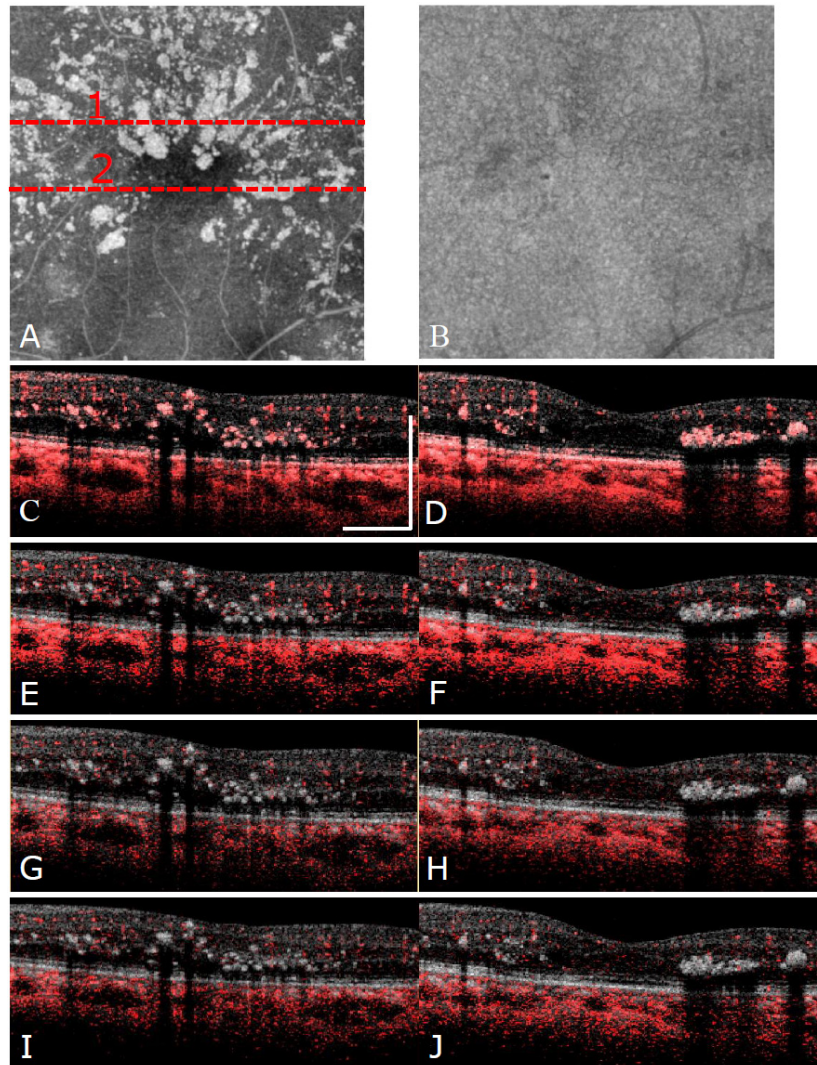


Fig. 2. (A) OCT structural projection image of the retinal tissue only (between ganglion cell layer and external limiting membrane) in the DR patient. (B) OCT structural projection image of the whole posterior eye including the choroid in the DR patient. (C)(E)(G)(I) and (D)(F)(H)(J) show the comparison between different methods (OMAG, wOMAG, CA1 and CA2, respectively) for detecting the blood flow in two typical B-scans at Line 1 and Line 2 as shown in (A). Structure is shown in grayscale and flow is shown in red. The scale bar in (C) indicates 500  $\mu\text{m}$ .

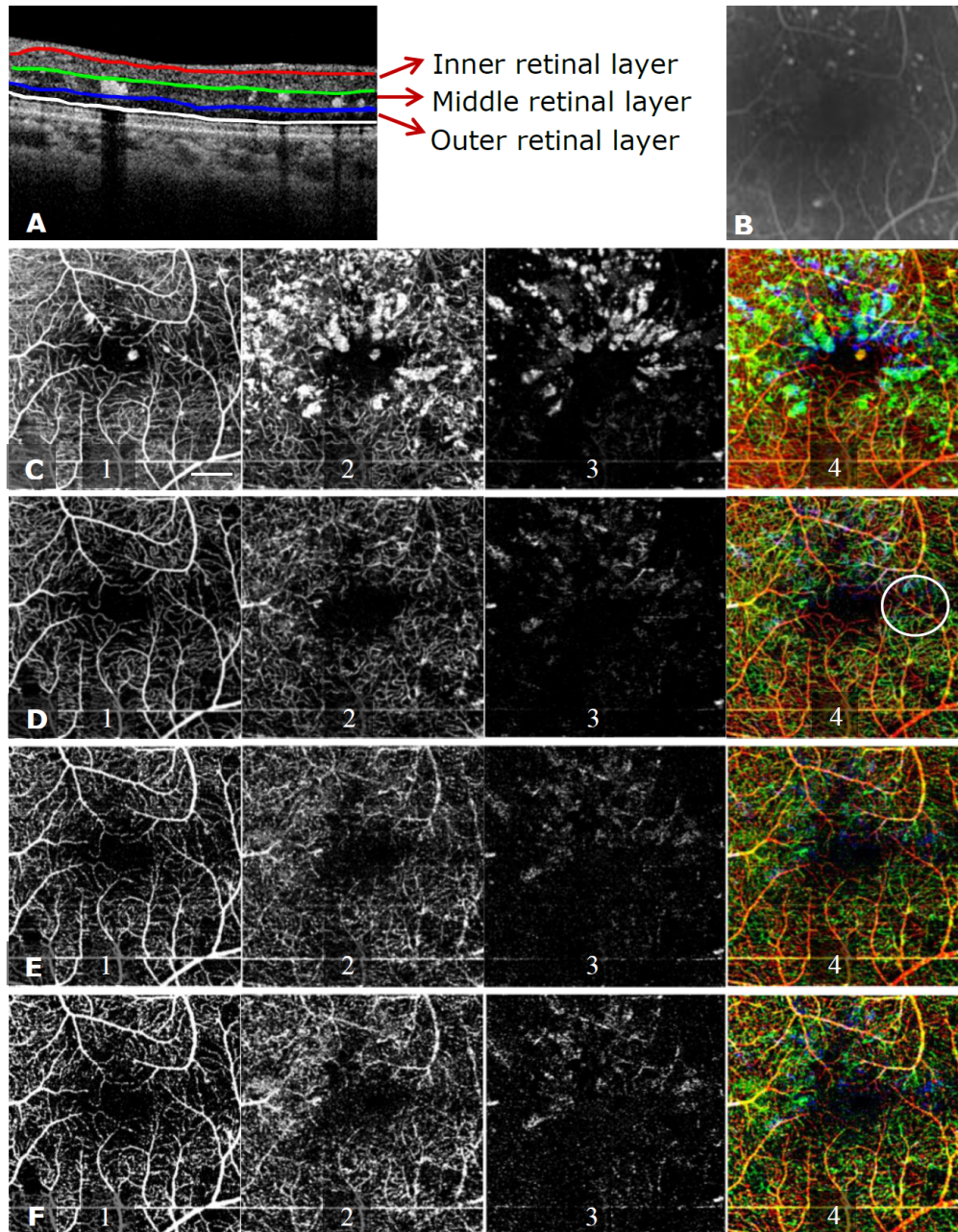


Fig. 3. (A) A schematic showing a typical segmentation of the three retinal layers based on the structural OCT image. (B) Zoomed FA corresponding to the OCT scanned region. (C)-(F) show the en face vascular images of the different layers using OMAG, wOMAG, CA1 and CA2, respectively. “1” stands for the inner retinal layer, “2” for the middle retinal layer, “3” for the outer retinal layer and “4” for a color coded display of the total retina with red indicating the inner retina, green for the middle retina and blue for the outer retina. The scale bar in (C1) indicates 500  $\mu\text{m}$  in both dimensions. In D4 the white circle shows the region where capillaries can be seen more clearly in wOMAG than others.

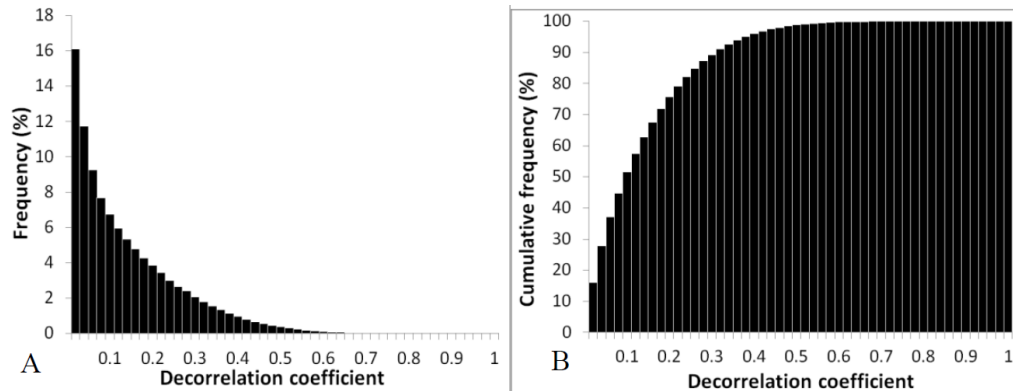


Fig. 4. (A) Frequency and (B) cumulative frequency histograms of the decorrelation coefficients in the scanned volume.

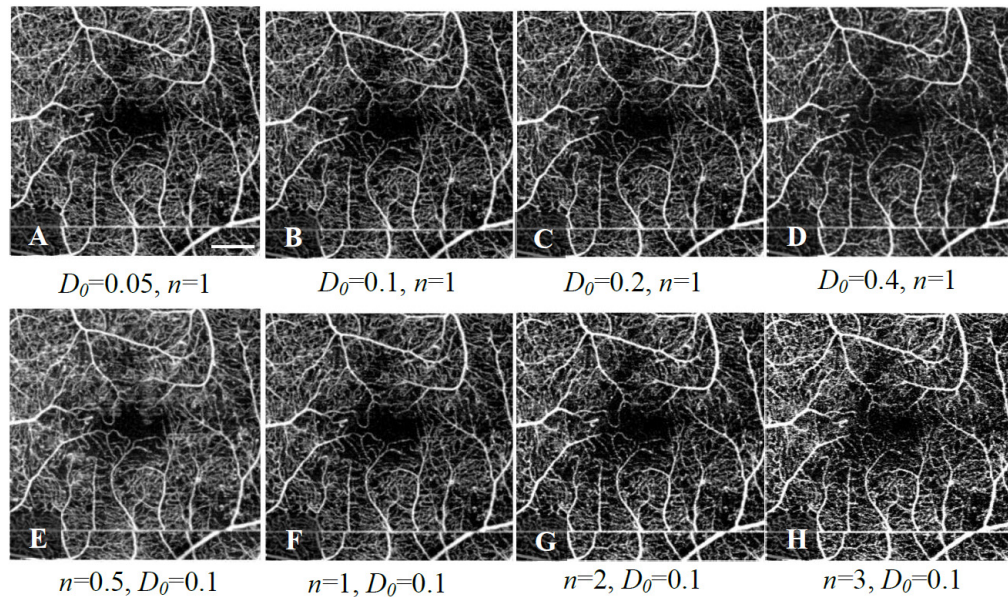


Fig. 5. (A)-(D) En face vascular imaging of the whole retina for different  $D_0$  (0.05, 0.1, 0.2, 0.4) while  $n = 1$ ; (E)-(H) En face vascular imaging of the retina for different  $n$  (0.5, 1, 2, 3) while  $D_0 = 0.1$ . The error bar in (A) indicates 500  $\mu\text{m}$ .

Results of OMAG and wOMAG in the left eye of the PCV patient are shown in Fig. 6. For this eye, most of the hyper-reflective foci in OCT image are located in the superior part of the image near the PCV. Similar to the DR patient, the hyper-reflection foci mainly exist in the middle and outer retinal layers. Compared with OMAG, the angiograms of wOMAG are mostly free of the hyper-reflective artifacts and give a clearer view of the capillary networks.

#### 4. Discussion

OMAG is a sensitive and effective method to detect functional capillary network in retina. However, the direct subtraction of OCT intensity signals among repeated B-scans in OMAG is prone to artifacts caused by hyper-reflective static tissues, which are commonly seen in patients with certain pathologies such as DR, AMD and PCV. In this study, a simple weighting method was proposed to suppress the hyper-reflection-induced artifacts in OMAG. An agar phantom study clearly showed the effectiveness of the proposed wOMAG method. Results of the case study in the DR patient demonstrated that compared to the other two OCT-

based angiography methods, the proposed method was superior in suppressing the artifacts while still maintaining a higher integrity of the detected capillary network in retina. The results obtained from the PCV patient further confirmed the effectiveness of the proposed method. Related topics of this study are discussed as follows.

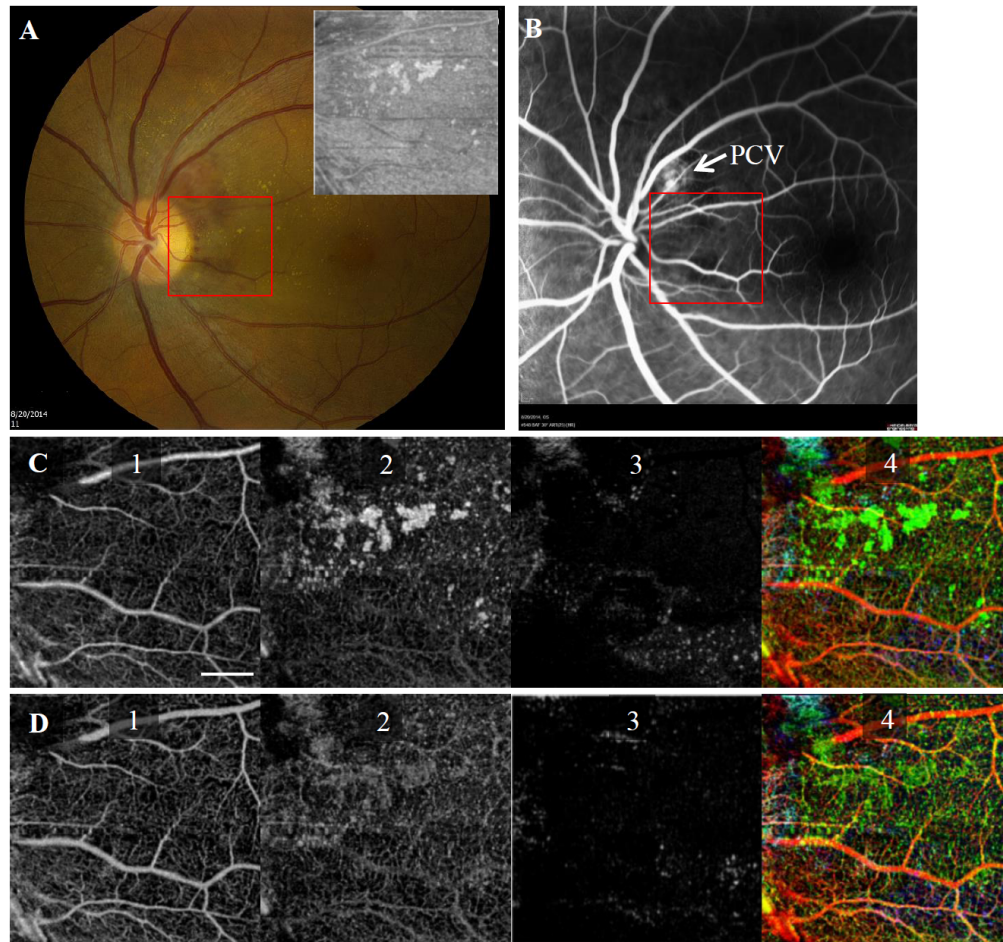


Fig. 6. (A) Color fundus image of the left eye (OS) in the PCV patient. A red rectangular window shows the region where OCT scan was performed. The inset at right upper corner shows the OCT structural en face image of the retina. (B) FA image of the scanned eye. Arrow shows where PCV exists and the red rectangular window shows the OCT scan region; (C) and (D) show the results obtained from OMAG and WOMAG without and with suppression of hyper-reflective artifacts. Refer to Fig. 3 for detailed explanation of 1-4 related to the color coding scheme. The scale bar in (C1) indicates 500  $\mu\text{m}$  in both dimensions.

#### 4.1. Hyper-reflection and DR

It is not unusual to observe scattered hyper-reflective foci in OCT images acquired from eyes with retinopathies including DR. It has been demonstrated in literature that there is no one-to-one correspondence among hyper-reflective spots observed in different imaging methods such as infrared fundus photograph, color fundus photograph, and OCT [24]. It is common that the hyper-reflective foci seen in OCT are not observed in other imaging methods. These foci may represent hard exudates or precursors of hard exudates, implying that OCT may be more sensitive to the detection of earlier retinal pathological changes than other modalities [35]. Constituents of the exudates are believed to mainly include lipid and proteins as extravasation

from the degraded blood-retinal barrier. Therefore, artifacts due to the hyper-reflective foci showing up in OMAG angiograms may not necessarily be useless. They clearly indicate that the vessels near the foci are most probably associated with degraded blood-retinal barrier. Hyper-reflective foci developing into the outer retina beyond ELM has been demonstrated to have a close relationship with the degradation of vision acuity [25]. Nevertheless, if the objective is to study the morphological information of vascular network itself, it is still necessary to develop suppression methods that can efficiently remove these artifacts for a clearer view of the microvascular circulation networks.

#### 4.2. Proposed suppression method for hyper-reflection artifacts

The artifacts induced by hyper-reflective static tissues are mainly caused by the high intensity of the OCT signal involved in the calculation of the flow signal using OMAG algorithms. Speckle in OCT is known to be multiplicative [27] and direct subtraction of the OCT intensity signals in the OMAG algorithm would make the results highly dependent on the intensity, i.e., signal to noise ratio (SNR) of the detected tissue [29]. In this study, we employed a weighted OMAG algorithm that utilizes a motion index, i.e. decorrelation coefficient, as an independent control variable to scale the OMAG flow signal so that the suppression of the artifacts is achieved. One advantage of choosing the decorrelation coefficient as the control variable is that it is a normalized value between 0 and 1 for convenient use. The decorrelation coefficient is used as an indicator of stability of the OCT signal. A smaller decorrelation coefficient more likely indicates that it is a static structural point so that the OMAG flow signal should be down-scaled to reduce the potential effects caused by hyper-reflection. On the other hand, if the decorrelation value is high, it more likely indicates a point with moving particles so that the OMAG flow-signal can be up-scaled correspondingly to enhance the detection of blood vessels. The image contrast is significantly increased in wOMAG compared to that of OMAG (for example, in terms of image contrast defined by a standard variation/mean of all pixels, it is 0.88 and 1.08 for Fig. 3(C1) and Fig. 3(D1), respectively). With respect to the weighting functions, two variables with a threshold value  $D_0$  and a nonlinear scaling factor  $n$  are used for controlling the magnitude of scaling. It was found that the change in  $D_0$  does not actually affect the image quality, which is due to the use of a logarithmic compression in displaying the final flow image. This log-operation converts multiplication into addition where different  $D_0$  only indicates the difference of a constant. Therefore, the effect of  $D_0$  can be removed by a proper thresholding in displaying the flow image. Through the histogram study  $D_0$  (Fig. 4), it is clear that no critical cutoff value can be used to differentiate the moving from the static tissues. Therefore, it is advantageous that no critical value of  $D_0$  is needed in obtaining optimal wOMAG images. In practical implementation, a typical threshold value such as  $D_0 = 0.1$  can still be used for wOMAG. However, it should be noted that a proper thresholding scheme is critical to generate the wOMAG images with good quality when different  $D_0$  is used. For the nonlinear factor  $n$ , it was demonstrated to achieve a good balance between artifact suppression and vessel smoothness (connectivity) when choosing a value between 1 and 2. A smaller value such as 0.5 cannot remove the artifacts well but a larger value such as 3 will make the vasculature network look disconnected with scattered bright spots, losing the smoothness of the network. This finding was quite consistent with statistical analysis for the decorrelation coefficients presented in Fig. 4, where no abrupt change of the frequency is observed. A constant change of the scaling function with the decorrelation coefficient would be better for the purpose of maintaining the visibility of blood vessel networks while suppressing the artifacts. It is uncertain whether the selected decorrelation coefficient is optimal as a control variable for scaling OMAG flow signal. In principle, any variable, free of hyper-reflection induced artifact can be incorporated in this scaled OMAG approach, such as the phase variance. Another related consideration is the computational complexity. The control variable should not impose high computational cost to overall system so that real time imaging is still

possible when this method is used in a clinical platform. The decorrelation coefficient used in the current study is computationally affordable. The search of an optimal control variable, however, warrants further investigations

#### 4.3. Comparison of different OCT angiography methods

The other two methods, i.e. log-intensity based speckle variance (CA1) and decorrelation coefficient (CA2) based OCT angiography, were also used to generate the enface vasculature images. CA1 can successfully suppress the artifacts induced by hyper-reflection because a logarithmic operation is firstly conducted before the calculation of variance, which reduces the effect of large baseline amplitude in computing the variance. In CA2, intensity normalization is conducted in calculating the decorrelation coefficient, leading to the suppression of the hyper-reflection effect. The enface vasculature images generated by these two methods were found to be quite similar. However, when compared to wOMAG, part of the capillary information is lost especially for vessels located within deeper retinal layers, as seen by less green vessels in the color-coded enface images (Fig. 3(D)-3(F)). The less visibility of capillary in CA1 and CA2 is believed to be caused by the uncontrolled nonlinear effect in the logarithmic or correlation analysis when the intensity of OCT signal becomes small. This can be understood by considering  $\log A - \log B = \log A/B$  and  $(A - B)^2/(A^2 + B^2)$ . In this case the result can be amplified with a small B from static structure or background noise. For the CA1 and CA2, the flow signal from static structure with a low intensity may be magnified, making it inseparable from that of capillaries. Although the amplification still can happen in the case of wOMAG, it is in a better controlled manner with the original OMAG signal as a baseline in scaling (Eq. (1)). Therefore, it has a better ability to maintain the visibility of the small blood vessels, i.e., the capillary network.

#### 4.4. Vascular imaging for detecting retinopathies

Due to the ability of wOMAG in the suppression of artifacts induced by hyper-reflection, the vascular network can be seen more clearly. From the vascular images, several morphological changes characteristic of pathologies such as DR can be identified, including capillary drop-out (arrows in Fig. 7(A)), capillary tortuosity or bypass (arrow head in Fig. 7(A)) and possible microaneurysms (diamond in Fig. 7(A)). With structural OCT images, additional pathologies such as edema (arrow in Fig. 7(B)) or pigment epithelial detachment (Fig. 7(D)) can be further observed, which would be helpful in a comprehensive diagnosis of the disease severity when combined with vascular images from wOMAG.

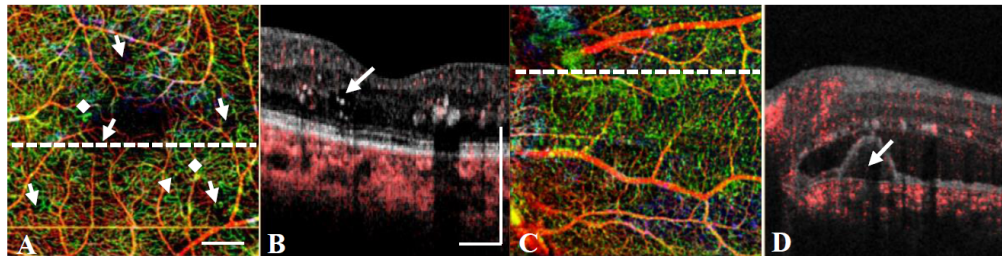


Fig. 7. (A) wOMAG of the left eye in the DR patient showing pathologies including capillary drop-out (arrows), tortuosity (arrowhead) and possible microaneurysm (diamond). (B) Structural OCT scanned at the dotted line of (A) showing the coexistence of an edema in the region with significant capillary dropout. (C) wOMAG of the left eye in the PCV patient. (D) Structural OCT scanned at the dotted line of (C) showing the existence of a pigment epithelial detachment below the hyper-reflective foci. The scale bar in (A) and (B) indicates 500  $\mu\text{m}$ .

#### 4.5. Potential applications

The proposed wOMAG is also useful in normal retina where the reflection of specific layers is strong, including the nerve fiber layer (NFL) and the RPE. For NFL, it is particularly thick

near the optic nerve disc so wOMAG can be applied to the disc region for a better observation of the vasculature and associated pathologies such as glaucoma. For RPE layer, the suppression of its artifacts may be useful for studying the choroidal vasculature, especially the choriocapillaris that is just beneath the RPE, which is otherwise inseparable without the suppression of hyper-reflective RPE. As discussed previously, hyper-reflection is commonly seen in quite a number of posterior eye pathologies including DR [24], AMD [26] and macular telangiectasia [36], and therefore the proposed wOMAG is also useful for the investigation of various ocular diseases.

## **5. Conclusions**

In this study, a weighted OMAG method is proposed to suppress the artifacts caused by hyper-reflection while optimally keeping the visibility and connectivity of the capillary network in OCT angiographic imaging. This method was demonstrated to be effective firstly in a phantom and then in two patients with the appearance of hyper-reflective foci in retina. Typical pathological changes such as capillary drop-out, tortuosity and microaneurysms associated with DR were successfully observed in wOMAG images after removing the artifacts. The proposed method is low cost in computation, which is important for clinical translation. Future study is currently being planned in a large cohort of patients with various retinopathies to test the clinical value of this method.

## **Acknowledgments**

This work was supported in part by the National Eye Institute (R01EY024158), a research grant from the Carl Zeiss Meditec, Inc., an unrestricted grant from Research to Prevent Blindness, and the Department of Bioengineering at the University of Washington.